Lawrence Berkeley National Laboratory
LBL Publications

Title
Structure and magnetism of Fe-doped BaSnO3 thin films

Permalink
https://escholarship.org/uc/item/0pf452mb

Journal
AIP Advances, 7(5)

ISSN
2158-3226

Authors
Alaan, Urusa S
N'Diaye, Alpha T
Shafer, Padraic
et al.

Publication Date
2017-05-01

DOI
10.1063/1.4977772

Peer reviewed

Structure and magnetism of Fe-doped BaSnO$_3$ thin films

Urusa S. Alaan, Alpha T. N'Diaye, Padraic Shafer, Elke Arenholz, and Yuri Suzuki

---

Structure and magnetism of Fe-doped BaSnO$_3$ thin films

Urusa S. Alaan,[1,2] Alpha T. N'Diaye,[3] Padraic Shafer,[3] Elke Arenholz,[3] and Yuri Suzuki[4]

[1]*Department of Materials Science and Engineering, Stanford University, Stanford, California 94305, USA*
[2]*Geballe Laboratory for Advanced Materials, Stanford University, Stanford, California 94305, USA*
[3]*Advanced Light Source, Lawrence Berkeley National Laboratory, Berkeley, California 94720, USA*
[4]*Department of Applied Physics, Stanford University, Stanford, California 94305, USA*

BaSnO$_3$ is an excellent candidate system for developing a new class of perovskite-based dilute magnetic semiconductors. In this study, we show that BaSn$_{0.95}$Fe$_{0.05}$O$_3$ can be grown from a background pressure of $\sim 2 \times 10^{-3}$ mTorr to oxygen pressures of 300 mTorr with high crystallinity and excellent structural quality. When grown in vacuum, the films may be weakly ferromagnetic with a nonzero x-ray magnetic circular dichroism signal on the Fe L$_3$ edge. Growth with oxygen flow appears to suppress magnetic ordering. Even for very thick films grown in 100 mTorr O$_2$, the films are paramagnetic. The existence of ferromagnetism in vacuum-grown BaSnO$_3$ may be attributed to the F-center exchange mechanism, which relies on the presence of oxygen vacancies to facilitate the ferromagnetism. However, other possible extrinsic contributions to the magnetic ordering, such as clusters of Fe$_3$O$_4$ and FeO or contamination can also explain the observed behavior. © *2017 Author(s). All article content, except where otherwise noted, is licensed under a Creative Commons Attribution (CC BY) license (http://creativecommons.org/licenses/by/4.0/).* [http://dx.doi.org/10.1063/1.4977772]

The discovery that dilute concentrations of magnetic impurities in a semiconducting matrix could lead to room-temperature ferromagnetism has been a tremendously exciting notion for the field of spintronics, the future of which relies on the development of new materials that can sustain both semiconducting behavior and spin polarization.[1,2] Progress in materials research of dilute magnetic semiconductors (DMS) such as (Cd,Mn)Te, (In,Mn)Sb, and (Ga,Mn)As has propelled intense interest in synthesizing so-called oxide-DMS, or O-DMS, materials that also may be transparent to visible light.[3–5] These systems include transition-metal-doped ZnO, TiO$_2$ (anatase), In$_2$O$_3$ and SnO$_2$.[6–8] In many cases, doping levels as low as 2-5% can induce a spontaneous moment at room temperature.[3,6]

One explanation for this long-range magnetic order was proposed by Coey *et al.* in 2003 for the SnO$_2$ system.[6] They hypothesized that the ferromagnetism in the Sn$_{0.95}$Fe$_{0.05}$O$_2$ system was a result of coupling between dopant sites that was facilitated by the presence of oxygen vacancies. Upon doping Fe^{3+} onto a Sn^{4+} site, they posited that compensation would result through the emergence of positively charged oxygen vacancies. Then, free electrons would become trapped at these sites, forming so-called "F-centers". The d-orbitals of the nearby Fe^{3+} dopants would then interact with each other through the trapped electron orbital with radius $a_0\varepsilon$, where a_0 is the Bohr radius and ε is the dielectric constant. Thus, each of the linked Fe^{3+} dopants would be antiferromagnetically aligned with the F-center, but ferromagnetically coupled to one another. In this way, a lightly doped transition-metal-doped compound could give rise to a spontaneous moment. The discrepancy between the predicted moment achieved by the F-center exchange mechanism and the lower experimentally observed moment was attributed to the presence of superexchange interactions, in which Fe^{2+} and Fe^{3+} dopants couple antiferromagnetically through a bridging oxygen anion.[6]

BaSnO$_3$ is a promising candidate for a transparent O-DMS.[9–12] It forms the perovskite structure *Pm-3m* with a lattice parameter of a=4.1163 Å (powder diffraction file 00-015-0780). When lightly doped to be n-type with La or Gd, it exhibits high room-temperature electron mobilities that have been attributed to the 5s character of the conduction band while also being transparent to visible light.[12–15] Recent reports have shown promise that BaSnO$_3$ can also be magnetically doped.[9,11,12,16,17] In some cases, transition-metal doping on the Sn site can lead to Curie temperatures exceeding 500 K, though doping with 3d transition metals invariably leads to highly insulating behavior.[10] Balamurugan *et al.* demonstrated that BaSn$_{1-x}$Fe$_x$O$_3$ (x=0.03, 0.04, 0.05) polycrystalline bulk samples exhibited hysteretic magnetization loops at room temperature, with Curie temperatures and magnetizations that decreased with increasing Fe-doping.[10] They suggested that Fe^{2+} dopants couple ferromagnetically via F-center exchange. To explain why the strength of the ferromagnetic signal decreased with higher levels of transition-metal-doping, they reasoned that the greater the concentration of Fe in the sample, the more likely it was for antiferromagnetic superexchange to occur at the expense of ferromagnetic exchange through F-centers.[10] In a later study, they showed that co-doping 1% W^{6+} and 4% Fe^{2+} onto the Sn^{4+} site led to even higher resistivities with a decrease in the magnetization, compared to samples that were doped with Fe only.[11] This was consistent with the F-center exchange mechanism, in that Fe$_{Sn}''$ may be compensated by W$_{Sn}^{\cdot\cdot}$ instead of V$_O^{\cdot\cdot}$.[26] A lower concentration of oxygen vacancies and corresponding F-centers would serve to suppress the net magnetization.

Thin films of BaSnO$_3$ doped with Fe and Mn have also exhibited room-temperature ferromagnetism.[16,17] The Fe-doped BaSnO$_3$ study by James *et al.* shows that with increasing amounts of Fe, the magnetization decreases while the opposite trend is observed by Balamurugan *et al.*[10,16] In each of these cases, the emergence of a spontaneous moment can be explained either by the F-center exchange mechanism (intrinsic ferromagnetism), or through contamination or clustering of the dopants (extrinsic ferromagnetism). If the F-center exchange mechanism applies to the transition-metal-doped BaSnO$_3$ system, then the magnetic moment per dopant should be enhanced by increasing levels of oxygen vacancies. We aimed to test this hypothesis by growing Fe-doped BaSnO$_3$ under a variety of oxygen pressures and determining the resulting magnetism.

In this study, we have grown iron-doped BaSnO$_3$ (BSFO) films at a series of oxygen pressures on (001) SrTiO$_3$ substrates. Pulsed laser deposition with a KrF laser ($\lambda = 248$nm) operating at a fluence of ~1.6 J/cm^2 was used to ablate a rotating sintered ceramic target with nominal stoichiometry BaSn$_{0.95}$Fe$_{0.05}$O$_3$. Samples were grown at 700°C with pressures ranging from 10^{-3} mTorr background pressure (no oxygen flow) to 300 mTorr O$_2$; the target-to-substrate distance was 3 inches. At these conditions, growth without oxygen flow in a background pressure of 2×10^{-3} mTorr is designated "Recipe A" and growth with an oxygen flow of 0.0425 mTorr O$_2$ will be referred to as "Recipe B". A second set of samples (designated "Recipe C") was grown at 750°C, a target-to-substrate distance of 2.5 inches, and 100 mTorr O$_2$. An X'Pert Panalytical x-ray diffractometer with a Cu Kα_1 source was used to obtain structural information and reciprocal lattice maps. Atomic force microscopy was conducted using a Digital Instruments Dimension 3100 instrument. Energy dispersive spectroscopy and a FEI XL30 Sirion scanning electron microscope with a field-emission gun source were used to confirm uniform spatial incorporation of the Fe dopant species. Bulk magnetometry of the film and substrate together were acquired with a Quantum Design Evercool Magnetic Property Measurement System. The Fe L$_{3,2}$ edges were probed using x-ray absorption spectroscopy and x-ray magnetic circular dichroism measurements at Beamlines 6.3.1 and 4.0.2 of the Advanced Light Source at Lawrence Berkeley National Laboratory. Total-electron-yield mode and a grazing incidence of 30° were used for these measurements.

Highly crystalline, epitaxial BaSn$_{0.95}$Fe$_{0.05}$O$_3$ thin films can be achieved at a range of different oxygen pressures, as shown in Figure 1. Undoped bulk BaSnO$_3$ has a lattice parameter of 4.1163 Å while SrTiO$_3$ has a lattice parameter of 3.905 Å; this large lattice mismatch of over 5% leads to complete film relaxation for films as thin as 25 nm as measured by reciprocal space maps (not shown), while still preserving film quality.[18,19] Each of the high-resolution θ-2θ scans (Figure 1a) grown in oxygen shows clear Laue oscillations around the 002 Bragg reflection, indicating excellent film quality on (001) SrTiO$_3$ substrates. The films grown without oxygen flow in a background pressure ~2×10^{-3} mTorr (labeled "vacuum" in Figure 1), exhibit a broadening of the film peak and a loss of well-defined oscillations. Aside from the 001 and 002 BaSnO$_3$ and SrTiO$_3$ reflections, no
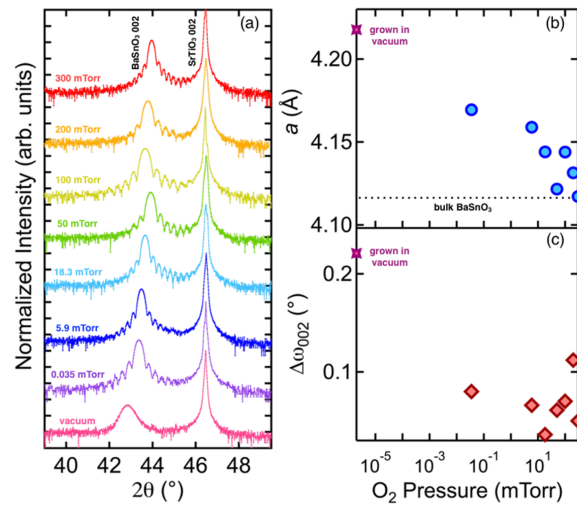
FIG. 1. X-ray diffraction results (on a logarithmic scale) for $BaSn_{0.95}Fe_{0.05}O_3$ films on (001) $SrTiO_3$ substrates grown at different oxygen pressures. (a) θ-2θ scans around the 002 Bragg reflection for films grown in 300, 200, 100, 50, 18.3, 5.9, and 0.035 mTorr of O_2 (from top to bottom). The bottom sample, labeled "vacuum", was grown without oxygen flow in a background pressure of $\sim$2$\times$10^{-3} mTorr. The intensities shown have been normalized by the substrate peak intensity for each film. (b) The corresponding out-of-plane lattice parameters a as calculated from the 002 reflection are given as a function of oxygen growth pressure on a logarithmic scale. (c) The full-width-at-half-maximum (FWHM) of the rocking curve around the 002 reflection is also plotted as a function of O_2 pressure during growth on a logarithmic scale.

other peaks are seen in the range 2θ=17-53° for any of these samples. In addition to being phase pure, ϕ-scans (not shown) confirm an epitaxial relationship between the film and substrate. When grown in low oxygen pressures, we may expect that more oxygen vacancies are likely to form. One indicator of oxygen-deficient films is an expansion of the lattice due to Coulombic repulsion arising from the presence of charged defects.[17] In Figure 1b, the lattice parameters of the films as a function of oxygen pressure are given. There is not a monotonic trend, though growth in very low oxygen pressures does seem to cause an enlargement of the unit cell. For a relative measure of crystalline quality, the full-width-at-half-maxima (FWHMs) of the rocking curves conducted on the 002 $BaSnO_3$ reflection are given in Figure 1c. All films have low FWHMs despite the large lattice mismatch, with the exception of the films grown in nominally vacuum atmosphere of $\sim$2$\times$10^{-3} mTorr. Thus, it is clear that in order to grow highly crystalline $BaSnO_3$ films, at least some oxygen flow is necessary when using the pulsed laser deposition technique. However, in terms of crystal quality, there is a wide range of oxygen pressures that can preserve both the crystallinity and phase purity of the compound.

Given that unit cell volume can be a proxy measurement for oxygen vacancy concentration in perovskite structure oxides, we chose to compare three sets of films with very different lattice constants. These sets are designated Recipes A, B, and C with the growth parameters mentioned earlier as well as in the Figure 2 caption, and the x-ray diffraction results of the films are given in Figure 2. The resulting lattice parameters for Recipes A, B, and C are 4.218 Å, 4.169 Å, and 4.119 Å, respectively. There is no difference between the lattice parameters of the thick and thin Recipe C samples.

SQUID magnetometry results taken at cryogenic temperatures are given in Figure 3 for the samples shown in Figure 2. In each case, there is a positive magnetization after background subtraction of the diamagnetic $SrTiO_3$ substrate. No samples exhibited room-temperature ferromagnetism. The film grown without oxygen flow (Recipe A), is weakly ferromagnetic below 60 K, with a saturation magnetization of approximately 0.8 μ_B/Fe (assuming a doping concentration of 5% Fe) and a coercivity of 420 Oe. For the film grown in 0.0425 mTorr O_2 (Recipe B), we observe a hysteresis in the magnetization below $\sim$70 K with a coercivity of 500 Oe. Finally, for recipe C, there is no hysteresis of the magnetization, and no magnetic remanence. The films are paramagnetic, and the shape is approximated by Brillouin functions assuming high spin Fe^{2+} and Fe^{3+} ions respectively
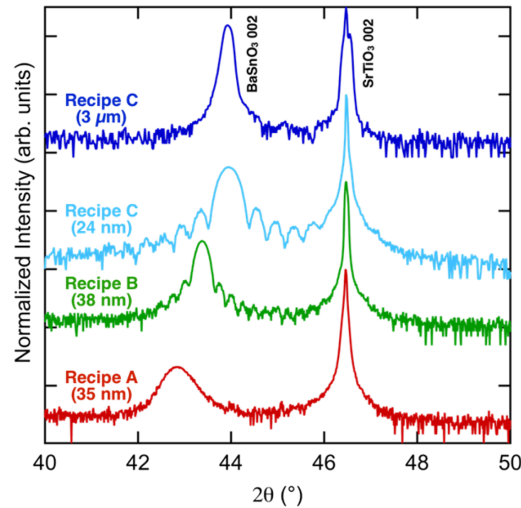
FIG. 2. X-ray diffraction θ-2θ scans around the 002 Bragg reflection for films grown using Recipes A, B and C to the indicated thicknesses. Intensity is plotted on a logarithmic scale and normalized by the 002 $SrTiO_3$ peak. Recipe A samples were grown at 700°C, a target-to-substrate distance of 3 inches, and a background pressure of 2×10^{-3} mTorr (no oxygen flow). Recipe B conditions were the same, but with an oxygen growth pressure of 0.0425 mTorr O_2. Both the thick and thin Recipe C samples were grown at 750°C, a target-to-substrate distance of 2.5 inches and an oxygen pressure of 100 mTorr. The lattice parameters for Recipes A, B, C (both thick and thin) were 4.218 Å, 4.169 Å, 4.119 Å, respectively.

as shown in Figure 3c. Even up to film thicknesses of 3 μm, there is no evidence of ferromagnetism in films grown under these conditions. It should also be noted that for the sample grown using Recipe B, the loop closes at about 2 kOe but does not appear to saturate until 35 kOe. This behavior could be the result of measuring a film with both paramagnetic and weak ferromagnetic contributions. A similarly-shaped magnetization curve is observed in Figure 3c for the Recipe C sample.

Using synchrotron radiation at the Advanced Light Source, we conducted x-ray absorption (XAS) and x-ray magnetic dichroism (XMCD) measurements in total-electron-yield mode for the sample grown using Recipe A (Figure 4). There is a weak, but definitive, x-ray absorption around the Fe $L_{3,2}$ edges. The Sn M_3 edge can be seen at approximately 714 eV. We were able to resolve an XMCD signal that switches signs when an opposite polarization of light is applied, indicating that the response is in fact a magnetic effect. The presence of a nonzero dichroism from the Fe $L_{3,2}$ edges confirms that iron is contributing to the net magnetization. We can use fingerprinting of Fe,[20–22] FeO,[23] α-Fe_2O_3,[22,24]
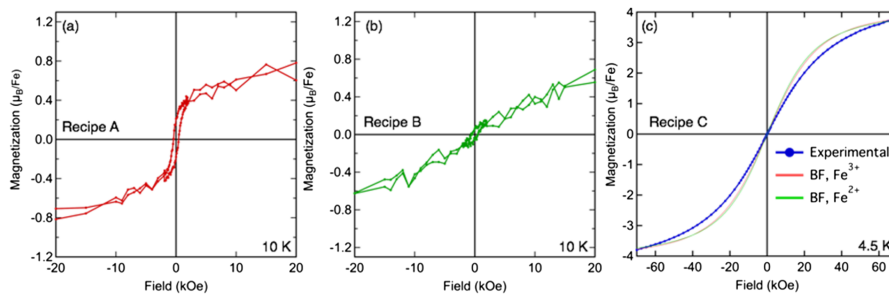

FIG. 3. Magnetization versus magnetic field loops as measured by SQUID magnetometry for samples grown using (a) Recipe A (no oxygen flow, 2×10^{-3} mTorr background pressure), (b) Recipe B (0.0425 mTorr O_2), and (c) Recipe C (100 mTorr O_2, thick film). In each case, the diamagnetic background from the substrate has been subtracted. All measurements were conducted after field-cooling in 70 kOe with the magnetic field oriented in the sample in-plane direction. For (a) and (b), the measurement was conducted at 10 K. In (c), the magnetization was measured at 4.5 K and the calculated Brillouin functions (BF) for high-spin Fe^{2+} and Fe^{3+} are also plotted.
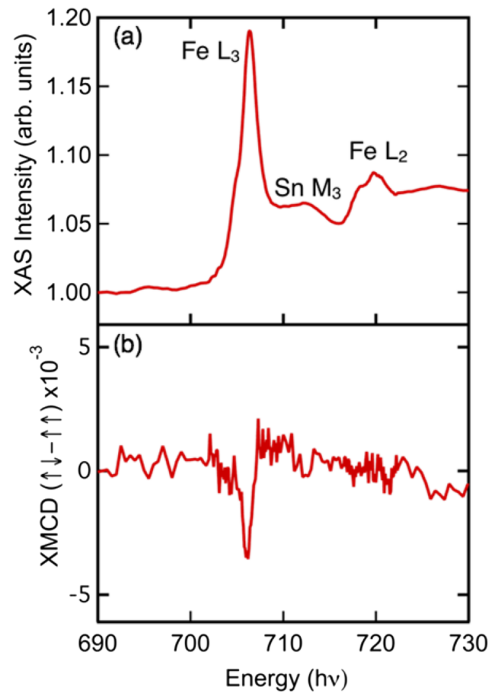
FIG. 4. (a) X-ray absorption and (b) x-ray magnetic circular dichroism spectra at the Fe $L_{3,2}$ edges for a ferromagnetic $BaSn_{0.95}Fe_{0.05}O_3$ sample grown using Recipe A (no oxygen flow, 2×10^{-3} mTorr background pressure). The small peak at 714 eV arises from the Sn M_3 edge. The measurements were conducted at 25 K with an applied magnetic field of 1.8 kOe.

γ-Fe_2O_3,[22–24] and Fe_3O_4[22,25] spectra to assess the Fe valence and coordination in our BSFO films. For α-Fe_2O_3, the Fe^{3+} cations are octahedrally coordinated, giving rise to a strong, narrow peak on the lower-energy-shoulder of the L_3 edge. We do not observe this feature in the BSFO films, implying that the iron dopants are not exclusively Fe^{3+}. This is in accordance with the suggestion by Balamurugan *et al.* that dopant centers in BSFO are Fe^{2+}.[10] γ-Fe_2O_3 reference spectra show a similar peak on the left-hand side of the main absorption edge that is suppressed from the α-Fe_2O_3 case due to mixture of octahedrally and tetrahedrally coordinated cations. This peak is also absent from our measurements. Fe and FeO spectra are qualitatively much more similar to the BSFO case, though neither take into account the broadening of the left-hand side of the peak. In the case of FeO, it is actually the right-hand side of the L_3 that shows a weak asymmetry. Finally, Fe_3O_4 reference spectra, like our films, have a bowing-out of the lower-energy side of the L_3 with a featureless right-hand side. Thus, there may be a mixture of Fe^{2+} and Fe^{3+} in the BSFO films, and/or Fe_3O_4 clusters which contribute to the ferromagnetism. However, since the Fe_3O_4 spectra shows even more of an asymmetry at the L_3 edge than the BSFO does, there may be additional be contributions from sources of Fe^{2+}, such as FeO.

All of the BSFO films are insulating, despite the aliovalent doping scheme of Fe^{2+} and Fe^{3+} on Sn^{4+} sites. This indicates that Fe_{Sn}'' and Fe_{Sn}' defects are compensated by $V_O^{\cdot\cdot}$ instead of conduction holes, as is common in oxides.[27] Oxygen vacancies may also mediate the F-center exchange mechanism, which is a possible cause for low-temperature ferromagnetic ordering in these BSFO films.

Though the observed ferromagnetism in films grown without oxygen could be attributed to F-center exchange, this is not the only possible explanation for the hysteretic signal. Clusters of iron and its related oxides can induce pockets of magnetically ordered material, leading to similar results as the ones we observe. In fact, it has been suggested in PLD studies of Fe-doped SnO_2 that the target stoichiometry may not match that of the film due to the volatility of Sn.[6] Such Sn loss results in films that are Fe-rich compared to Sn.[6] If this is the case, then in our films, the presence of excess Fe could lead to clustering (e.g. of Fe_3O_4) and the net magnetic moment may arise from these extrinsic factors.

Since changing the PLD target-to-substrate distance can preferentially impact the incorporation of volatile elements, we may induce a stoichiometric change that is not a direct result of anion vacancies by reducing the distance from 3 inches (Recipe A&B) to 2.5 inches (Recipe C). A difference in cation stoichiometry could also change the lattice parameter. Thus, the differences between the high-pressure-grown and low-pressure-grown samples are likely subtler than simple differences in the oxygen vacancy concentrations. Furthermore, our XAS results suggest that Fe_3O_4 or FeO may be present in the ferromagnetic samples. While we see no evidence for non-$BaSnO_3$ phases in the XRD results of Figures 1 and 2, our SQUID magnetometry results may also support a hypothesis of Fe_3O_4 or FeO clusters. The samples grown with Recipes A and B show a low net magnetic moment per iron dopant, and the presence of clusters with antiferromagnetic ordering would cause a suppression of the net magnetization. For comparison, we also grew a thick film ($\sim$1.4 μm) following the conditions of Recipe A (not depicted). The magnetization does not exhibit hysteresis and the x-ray diffraction shows evidence of multiple phases. This suggests that perhaps the ferromagnetism that is observed in thinner films may be due to dopant clustering or contamination.

It must also be noted that though previous studies on Fe-doped $BaSnO_3$ have shown room-temperature ferromagnetism, we do not find any evidence of long-range magnetic ordering at such temperatures in any of our samples.[10,11,16] This could suggest that our films do *not* have clustering of iron or iron oxides (which have ordering temperatures well above 300 K), that the ferromagnetism we observe is from an intrinsic mechanism such as F-center exchange, and that in cases where high-temperature ferromagnetism is observed, the signal may actually be extrinsic in nature. Another possibility is that dopant clustering is responsible in all cases, but that in our films the clusters are small or well-separated enough to severely impede long-range coupling between Fe sites.

In summary, we have found that high-quality, epitaxial $BaSn_{0.95}Fe_{0.05}O_3$ films can be grown under a wide range of oxygen pressures and conditions by pulsed laser deposition, and different growth conditions can induce paramagnetism, and possibly ferromagnetism. Together these results indicate that the ferromagnetic signal may be attributed to the presence of ferrimagnetic Fe_3O_4 clusters or contamination in addition to the F-center exchange mechanism.

ACKNOWLEDGMENTS

[1] S. A. Wolf, D. D. Awschalom, R. A. Buhrman, J. M. Daughton, S. von Molnár, M. L. Roukes, A. Y. Chtchelkanova, and D. M. Treger, Science **294**, 1488 (2001).
[2] H. Katayama-Yoshida and K. Sato, Phys. B Condens. Matter **327**, 337 (2003).
[3] J. M. D. Coey and S. A. Chambers, MRS Bull. **33**, 1053 (2008).
[4] H. Chou, C. P. Lin, J. C. A. Huang, and H. S. Hsu, Phys. Rev. B - Condens. Matter Mater. Phys. **77**, 1 (2008).
[5] V. A. Ivanov, O. N. Pashkova, E. A. Ugolkova, V. P. Sanygin, and R. M. Galéra, Inorg. Mater. **44**, 1041 (2008).
[6] J. M. D. Coey, A. P. Douvalis, C. B. Fitzgerald, and M. Venkatesan, Appl. Phys. Lett. **84**, 1332 (2004).
[7] R. Seshadri, Curr. Opin. Solid State Mater. Sci. **9**, 1 (2005).
[8] N. H. Hong, J. Sakai, N. Poirot, and V. Brizé, Phys. Rev. B - Condens. Matter Mater. Phys. **73**, 3 (2006).
[9] K. Balamurugan, N. Harish Kumar, B. Ramachandran, M. S. Ramachandra Rao, J. Arout Chelvane, and P. N. Santhosh, Solid State Commun. **149**, 884 (2009).
[10] K. Balamurugan, N. H. Kumar, J. A. Chelvane, and P. N. Santhosh, J. Alloys Compd. **472**, 9 (2009).
[11] K. Balamurugan, N. Harish Kumar, J. Arout Chelvane, and P. N. Santhosh, Phys. B Condens. Matter **407**, 2519 (2012).
[12] U. S. Alaan, P. Shafer, A. T. N'Diaye, E. Arenholz, and Y. Suzuki, Appl. Phys. Lett. **108**, 42106 (2016).
[13] H. Mizoguchi, H. W. Eng, and P. M. Woodward, Inorg. Chem. **43**, 1667 (2004).
[14] H. J. Kim, U. Kim, H. M. Kim, T. H. Kim, H. S. Mun, B. G. Jeon, K. T. Hong, W. J. Lee, C. Ju, K. H. Kimy, and K. Char, Appl. Phys. Express **5**, 8 (2012).
[15] S. Sallis, D. O. Scanlon, S. C. Chae, N. F. Quackenbush, D. A. Fischer, J. C. Woicik, J.-H. Guo, S. W. Cheong, and L. F. J. Piper, Appl. Phys. Lett. **103**, 42105 (2013).
[16] K. K. James, A. Aravind, and M. K. Jayaraj, Appl. Surf. Sci. **282**, 121 (2013).

[17] Q. Liu, Y. He, H. Li, B. Li, G. Gao, L. Fan, and J. Dai, Appl. Phys. Express **7**, 33006 (2014).

[18] A. J. Smith and A. J. E. Welch, Acta Crystallogr. **13**, 653 (1960).

[19] P. H. Borse, U. A. Joshi, S. M. Ji, J. S. Jang, J. S. Lee, E. D. Jeong, and H. G. Kim, Appl. Phys. Lett. **90**, 1 (2007).

[20] C. Chen, Y. Idzerda, H.-J. Lin, N. Smith, G. Meigs, E. Chaban, G. Ho, E. Pellegrin, and F. Sette, Phys. Rev. Lett. **75**, 152 (1995).

[21] J. Stöhr and H. C. Siegmann, *Magnetism: From Fundamentals To Nanoscale Dynamics* (Springer, 2006).

[22] D. Nolle, E. Goering, T. Tietze, G. Schütz, A. Figuerola, and L. Manna, New J. Phys. **11**, 33034 (2009).

[23] H. J. Lee, G. Kim, D. H. Kim, J.-S. Kang, C. L. Zhang, S.-W. Cheong, J. H. Shim, S. Lee, H. Lee, J.-Y. Kim, B. H. Kim, and B. I. Min, J. Phys. Condens. Matter **20**, 295203 (2008).

[24] J. Y. Kim, T. Y. Koo, and J. H. Park, Phys. Rev. Lett. **96**, 47205 (2006).

[25] R. Kumar, R. J. Choudhary, M. W. Khan, J. P. Srivastava, C. W. Bao, H. M. Tsai, J. W. Chiou, K. Asokan, and W. F. Pong, J. Appl. Phys. **97**, 93526 (2005).

[26] Here we employ Kröger-Vink notation to illustrate charge compensation, where Fe_{Sn}'' refers to Fe^{2+} cations on Sn^{4+} sites (defects each with a charge of -2), $W_{Sn}^{\cdot\cdot}$ refers to W^{6+} cations on Sn^{4+} sites (defects each with a charge of +2), and $V_O^{\cdot\cdot}$ refers to oxygen vacancies (which each carry a +2 charge). Fe_{Sn}'' defects are deliberately introduced in this case, and may be compensated by $W_{Sn}^{\cdot\cdot}$ or $V_O^{\cdot\cdot}$.

[27] We again employ Kröger-Vink notation, where Fe_{Sn}'' refers to Fe^{2+} cations on Sn^{4+} sites (defects each with a charge of -2), Fe_{Sn}' refers to Fe^{3+} cations on Sn^{4+} sites (defects each with a charge of -1), and $V_O^{\cdot\cdot}$ refers to oxygen vacancies (which each carry a +2 charge).